CLM-P826

CLM-P826

Toroidal Internal Kink Stability in Tokamaks with Ultra Flat q profiles

R. J. Hastie
T. C. Hender

UK ATOMIC ENERGY AUTHORITY

Culham Laboratory

CLM-P826

Toroidal Internal Kink Stability in Tokamaks with Ultra Flat q profiles

R.J. Hastie and T.C. Hender

Culham Laboratory, Abingdon, Oxon. OX14 3DB, England
(UKAEA/Euratom Fusion Association)

Abstract

Linear stability properties of the ideal internal kink mode in toroidal geometry are calculated for equilibria in which the $q(r)$ profile is very flat and $q \approx 1$ in the core region of the plasma. Marginal stability criteria and growth rates are calculated analytically in the large aspect ratio limit and compared with numerical results from the FAR code. The theory is developed for $m = n = 1$ modes and for higher $m(=n)$ modes. The temperature perturbation due to adiabatic expansion in the linear phase of the 1/1 mode is calculated and compared with experimental data, showing that the prediction from ideal mhd theory cannot account for the observed temperature increase on JET. Comparison with collisionless theory suggests that the observed temperature increase can be accounted for by compression of the trapped particles.

(Submitted for publication in NUCLEAR FUSION)

Culham Laboratory
United Kingdom Atomic Energy Authority
Abingdon
Oxfordshire OX14 3DB

July, 1987

1. Introduction

Observations of the initial plasma displacement during the sawtooth collapse in JET discharges [1,2] show that the radial displacement eigenfunction $\xi_r(r)$ is not close to the Heaviside function

$$\xi_r = 1 \qquad 0 \leq r \leq r_1$$
$$= 0 \qquad r > r_1 \tag{1}$$

which is usually predicted by analytic theory (and computations) of internal kink modes, when $q(r_1) = 1$.

The analytic theories of Bussac et al [3] (for a single $q = 1$ surface) and of Hastie et al [4] (for multiple $q = 1$ surfaces) both assume $|q - 1| >> \varepsilon = \frac{a}{R}$ in the inner region. However, computations[2,4]of the internal kink mode for ultra flat $q(r)$, with $|q(r) - 1| \leq \varepsilon$ in $[0, r_1]$ show approximately parabolic $\xi_r(r)$ corresponding to convective flows of the type seen in JET.[2] This gives support to Wesson's suggestion [2,5] that, at the moment of sawtooth collapse, and indeed throughout the whole sawtooth cycle, $q \simeq 1 + 0(\varepsilon)$ in the region $r \leq r_1$.

In Section 2 of this paper the analytic theory of the toroidal ideal internal kink mode is developed for equilibria of this type. Analytic expressions for the eigenfunction $\underset{\sim}{\xi}(r)$ are obtained and shown to depend

on both the pressure profile $p(r)$ and the q profile $\delta q(r) \equiv q(r) - 1$. Expressions are also obtained for the marginal stability criterion. Similar analytic results are derived for the shorter wavelength modes with $m = n = 2, 3, 4$ etc. In Section 3 expressions for the growth rates of $m/n = 1$ modes are obtained and the $1/1$ growth rates are compared with numerical results obtained from the FAR stability code[4,6]. Section 4 is devoted to a comparison of the theoretically predicted compressional heating during the linear phase of the $m = n = 1$ ideal kink mode with that observed experimentally during sawtoothing in JET. It is found that ideal MHD theory fails (by two orders of magnitude) to predict the observed temperature rise. In Section 5 we investigate collisionless stability theory[7,8] and show how the temperature increase can be accounted for by the compression of trapped electrons. Collisionless theory requires a modification of the ideal mhd stability boundaries for the $m/n = 1$ modes investigated in the previous sections. The modified stability boundary of the $1/1$ mode is calculated in Section 6. We conclude with a discussion of the revised stability thresholds.

2. Minimisation of δW for a large aspect ratio equilibrium

In this section we consider the order by order minimisation of the energy integral

$$\delta W = \frac{1}{2} R_0 B_0{}^2 \int r\, dr\, d\theta d\phi \left\{ \left| \frac{1}{r} \frac{\partial}{\partial r} (r\xi_r) + \frac{1}{r} \frac{\partial}{\partial \theta} \xi_\theta \right|^2 \right.$$

$$+ \frac{1}{R_0{}^2} \left| r\nabla\theta \left(\frac{\partial \xi_r}{\partial \phi} + \frac{1}{q} \frac{\partial \xi_r}{\partial \theta} \right) + \nabla r \left(\frac{\partial}{\partial r} \left(\frac{r\xi_r}{q} \right) - \frac{\partial \xi_\theta}{\partial \phi} \right) \right|^2$$

$$+ \frac{g'}{fR_0} \left[|\xi_r|^2 r \left(\frac{1}{q} \right)' + \xi_\theta \left(\frac{\partial}{\partial \phi} + \frac{1}{q} \frac{\partial}{\partial \theta} \right) \xi_r{}^* + \xi_\theta{}^* \left(\frac{\partial}{\partial \theta} + \frac{1}{q} \frac{\partial}{\partial \theta} \right) \xi_r \right]$$

$$\left. + \frac{p'}{fR_0{}^3 B_0{}^2} \left[\frac{1}{r} \frac{\partial}{\partial r} \left(\frac{R^2 |\xi_r|^2 r^2}{gq} \right) + \frac{R^2}{g} \left(\xi_\theta \frac{\partial \xi_r{}^*}{\partial \phi} + \xi_0{}^* \frac{\partial}{\partial \phi} \xi_r \right) \right] \right\} \qquad (2)$$

The equilibrium magnetic field is given by

$$\underset{\sim}{B} = R_0 B_0 \left(f(r) \nabla\phi \times \nabla r + g(r) \nabla\phi \right) \qquad (3)$$

and the r, θ, ϕ coordinates are those used in references [3] and [9].

We consider an equilibrium in which

$$|q(r) - 1| \lesssim 0(\varepsilon) \quad \text{for} \quad 0 < r < r_1$$

while $q(r)$ increases from near unity at r_1 to $q_a \gtrsim 2$ at the edge of the plasma $(r = a)$.

The situation of interest is that in which $q(r) > 1$ at all radii, since we expect that a marginally stable equilibrium will always exist before q can evolve down to unity at any radius.

Returning to δW we insert the expansion

$$\underset{\sim}{\xi} = \underset{\sim}{\xi}_0 + \varepsilon \underset{\sim}{\xi}_1 + \varepsilon^2 \underset{\sim}{\xi}_2$$

where $\underset{\sim}{\xi}_0 = \underset{\sim}{\xi}_0(r)\, e^{i(m\theta - n\phi)}$ with $m = n$ and the explicit expansion of the equilibrium quantities [9]

$$R^2 = R_0^2\left[1 - 2\frac{r}{R_0}\cos\theta - 2\frac{\Delta}{R_0} - r\frac{\Delta'}{R_0} - \frac{1}{2}\frac{r^2}{R_0^2}\right] \tag{4}$$

$$|\nabla r|^2 = 1 - 2\Delta'\cos\theta + \frac{1}{2}\Delta'^2 + \frac{3}{4}\frac{r^2}{R_0^2} + \frac{\Delta}{R_0} \tag{5}$$

$$r\nabla r \cdot \nabla\theta = \left(r\nabla'' + \Delta' + \frac{r}{R_0}\right)\sin\theta \tag{6}$$

$$r^2|\nabla\theta|^2 = 1 + 2\left(\Delta' + \frac{r}{R_0}\right)\cos\theta + \frac{3}{2}\left(\Delta' + \frac{r}{R_0}\right)^2 + \frac{1}{4}\frac{r^2}{R_0^2} + \frac{\Delta}{R_0^2} + \frac{\Delta'^2}{2} + \frac{1}{2}\left(r\Delta'' + 2\Delta' + \frac{r}{R_0}\right)\left(r\Delta'' + \frac{r}{R_0}\right) \tag{7}$$

$$f = f_1 + \varepsilon^2 f_3 +$$

$$g = 1 + \varepsilon^2 g_2 + \varepsilon^4 g_4 + \qquad (8)$$

$$p = \varepsilon^2 p_2 + \varepsilon^4 p_4 +$$

where $\Delta(r)$ is the toroidal shift, and ε labels small terms for convenience

In leading order (which we label δW_{-2}) we find

$$\delta W_{-2} = 2\pi^2 R_0 B_0{}^2 \int_0^a \frac{dr}{r} \left| \frac{\partial}{\partial r} (r\xi_{r0}) + im\xi_{\theta 0} \right|^2 \qquad (9)$$

This vanishes when

$$\xi_{\theta 0} = \frac{i}{m} \frac{d}{dr} (r\xi_{r0}) \qquad (10)$$

In next order

$$\delta W_0 = 2\pi^2 R_0 B_0{}^2 \int_0^a \frac{dr}{r} \left| \frac{\partial}{\partial r} (r\xi_{r1}) + \frac{\partial}{\partial \theta} \xi_{\theta 1} \right|^2$$

$$+ 2\pi^2 R_0 B_0{}^2 \int_{r_1}^a r dr \left(\frac{1}{q} - 1\right)^2 \left[\left| r \frac{d\xi_{r0}}{dr} \right|^2 + (m^2 - 1) |\xi_{r0}|^2 \right] \qquad (11)$$

This expression also vanishes when,

$$\frac{\partial \xi_{\theta 1}}{\partial \theta} + \frac{\partial}{\partial r}\left(r \xi_{r1}\right) = 0 \qquad (12)$$

and $\xi_{r0}(r) = 0 \qquad r_1 < r \leq a.$

We note that, because the factor $\left(\frac{1}{q} - 1\right)^2 \sim 0(\varepsilon)^2$ in the range $[0, r_1]$, no information about $\xi_{r0}(r)$ in $[0, r_1]$ has been obtained, other than the boundary condition

$$\xi_{r0}(r_1) = 0 \qquad (13)$$

The radius r_1 which bounds the plasma core region in which $|q - 1| \lesssim \varepsilon$ does not have a precisely defined value. Physically meaningful results for stability thresholds, growth rates etc., must of course be independent of the choice of r_1. This will be achieved by regarding r_1 as a parameter to be varied in the minimisation of $\delta W(\underline{\xi}, \underline{\xi})$, or the maximisation of the growth rate γ.

Proceeding to next order we find

$$\delta W_2 = 2\pi^2 \frac{B_0^2}{R_0} \int_0^{r_1} r dr \left\{ \left(\frac{1}{q} - 1\right)^2 \left[\left| \frac{r d\xi_{r0}}{dr} \right|^2 + (m^2-1) |\xi_{r0}|^2 \right] + 2 \left(\frac{Rp'}{B_0^2}\right)^2 |\xi_{r0}|^2 \right.$$

$$- \frac{Rp'}{B_0^2} \left[\xi_{r0}^* \left(\frac{r}{m+1} \frac{d\xi_{r1}^{(m+1)}}{dr} + \frac{(m+2)}{(m+1)} \xi_{r1}^{(m+1)} - \frac{r}{m-1} \frac{d\xi_{r1}^{(m-1)}}{dr} + \frac{m-2}{m-1} \xi_{r1}^{(m-1)} + c.c. \right) \right]$$

$$+ 2\pi^2 \frac{B_0^2}{R} \int_0^a r dr \left\{ \left(\frac{1}{q} - \frac{n}{m+1}\right)^2 \left[\left| r \frac{d\xi_{r1}^{(m+1)}}{dr} \right|^2 + m(m+2) |\xi_{r1}^{(m+1)}|^2 \right] \right.$$

$$\left. \left. + \left(\frac{1}{q} - \frac{n}{m-1}\right)^2 \left[\left| r \frac{d\xi_{r1}^{(m-1)}}{dr} \right|^2 + m(m-2) |\xi_{r1}^{(m-1)}|^2 \right] \right\} \qquad (14)$$

Stability is determined in this order by the minimisation of δW_2 with respect to ξ_{r0}, and the two sideband displacements $\xi_1^{(m\pm1)}$ which are $O(\varepsilon)$ smaller than ξ_0, and are driven by toroidal coupling. The boundary conditions require

$$\xi_{r0} \to 0 \qquad \text{as } r \to r_1+$$

and $\xi_{r1}^{(m\pm1)}$ to be the small solutions at their respective singular surfaces, $q = 1 \pm \frac{1}{m}$, if such exist, or $\xi_{r1}^{(m\pm1)}(a) = 0$ if the singular surface is not present.

In the region $[r_1, a]$ only $\xi_{r1}^{(m\pm1)}$ appear in δW_2 and the usual cylindrical Euler equations are obtained

$$\frac{d}{dr}\left[r^3\left(\frac{1}{q}-\frac{n}{m\pm1}\right)^2\frac{d\xi_{r1}^{(m\pm1)}}{dr}\right]-m(m\pm2)r\left(\frac{1}{q}-\frac{n}{(m\pm1)}\right)^2\xi_{r1}^{(m\pm1)}=0 \qquad (15)$$

In the inner region $[0,r_1]$ the minimising Euler equations form a sixth order system. Here we take $\frac{1}{q}-\frac{n}{m\pm1}\simeq\frac{\pm1}{(m\pm1)}$ and write $q-1=\delta q(r)$. The appropriate equations are

$$\frac{d}{dx}\left[x^3\delta q^2\frac{d\xi_0}{dx}\right]+x\xi_0\left[(m^2-1)\delta q^2+\frac{\alpha^2}{2}\right]+\frac{\alpha}{2(m+1)}x^{-m}\frac{d}{dx}\left[\xi_1^{(m+1)}x^{m+2}\right]$$

$$-\frac{\alpha}{2(m-1)}x^m\frac{d}{dx}\left[\xi_1^{(m-1)}x^{2-m}\right]=0 \qquad (16)$$

$$\frac{d}{dx}\left[x^{-2m-1}\frac{d}{dx}\left(\xi_1^{(m+1)}x^{m+2}\right)\right]=\frac{(m+1)}{2}\frac{d}{dx}\left[\alpha\xi_0x^{-m}\right] \qquad (17)$$

$$\frac{d}{dx}\left[x^{2m-1}\frac{d}{dx}\left(\xi_1^{(m-1)}x^{2-m}\right)\right]=-\frac{(m-1)}{2}\frac{d}{dx}\left[\alpha\xi_0x^m\right] \qquad (18)$$

where $\alpha=2Rp'/B_0^2$, $x=r/r_1$, and we have dropped the subscript r on ξ_0 and ξ_1 for simplicity.

We may integrate Eqs. (17) and (18) to eliminate the sideband displacements $\xi_1^{(m\pm1)}$ from Eq. (16) and obtain an integro-differential eigenvalue equation for ξ_0;

$$\frac{d}{dx}\left\{x^3\delta q^2\frac{d\xi_0}{dx}\right\}-\xi_0x(m^2-1)\delta q^2+\alpha x^{m+1}\Lambda_m\int_0^1\alpha\,x^{m+1}\xi_0dx=0 \qquad (19)$$

where

$$\Lambda_m = \frac{(m+1)}{2} \frac{(C_m + m + 2)}{(m - C_m)} \tag{20}$$

with $C_m = \dfrac{x\xi_1^{(m+1)}}{\xi_1^{(m+1)}}$ $(x=1)$, evaluated from the solution of Eq. (15) which vanishes at $r=a$, or is small at $q = \dfrac{m+1}{n}$ if this resonant surface is within the plasma.

(a) The m=n=1 mode

The singularities which arise in Eq. (16) when $m=1$ are only apparent since the radial displacement of the lower sideband $\xi_{r1}^{(0)}$ vanishes. A separate treatment of this case reproduces Eqs. (19) and (20) with $m=1$. The eigenvalue Eq. (19) is then easily solved for arbitrary profiles $\alpha(x)$, $\delta q(x)$ to obtain the stability condition and eigenfunction for the $m=n=1$ mode;

$$\int_0^1 \alpha\, x^2 [I(1) - I(x)]dx < \frac{1-C_1}{C_1+3} \tag{21}$$

with

$$I(x) = \int_0^x \frac{ds}{s^3 \delta q^2} \int_0^s \alpha(t) t^2 dt \tag{22}$$

$$\xi_0(x) = \xi_0\left(1 - I(x)/I(1)\right) \tag{23}$$

For the simple case of a parabolic pressure profile

$$p = p_0\left(1 - \frac{r^2}{r_0^2}\right) \qquad \text{for } 0 \leq r \leq r_1 \tag{24}$$

and constant safety factor

$$q-1 = \delta q = \text{constant} \qquad 0 \leq r \leq r_1 \tag{25}$$

the stability criterion becomes

$$\delta q > \beta_0 \frac{Rr_1}{r_0^2}\left[\frac{C+3}{24(1-C)}\right]^{1/2} \tag{26}$$

(b) <u>The $m=n\geq 2$ modes</u>

For the simple choice of profiles defined by Eqs. (24) and (25) the eigenvalue equation (19) can also be solved for general m, to obtain the stability criterion for higher m modes. This is :-

$$\delta q > \beta_0 \frac{Rr_1}{r_0^2}\left[\frac{C_m+m+2}{4(m+1)(m+2)(m-C_m)}\right]^{1/2} \tag{27}$$

which agrees in the appropriate limit with expression (26). The values of C_m have been determined numerically for the profile

$$q = 1 + 3\left(\frac{r-r_1}{a}\right)^2 \quad ; \quad \frac{r_1}{a} = \frac{1}{3} \quad \text{for} \quad r_1 \leq r \leq a.$$

and the dependence of the threshold β_0 on the mode number m is shown in Fig 1. As in the case of cylindrical geometry (P. Kirby [10]) the m=1 stability boundary occurs at a lower value of β_0 than the boundaries for higher (m,n) modes.

3. Growth Rates of Internal modes with m/n = 1

To evaluate growth rates we equate the kinetic energy

$$\frac{\gamma^2}{\gamma_A^2} K = 2\pi^2 \frac{B_0^2}{R_0} \frac{\gamma^2}{\gamma_A^2} \int_0^{r_1+} r dr \, |\xi|^2 \tag{28}$$

to the potential energy, including the compressional part

$$\delta W_{2c} = 2\pi^2 B_0^2 R_0 \int_0^{r_1} r dr \, \frac{\Gamma p}{B_0^2} \, |\nabla \cdot \xi|^2 \tag{29}$$

where Γ is the adiabatic index.

The growth rate is then determined from [11]

$$\frac{\gamma^2}{\gamma_A^2} = \underset{\xi}{\text{maximum}} \left\{ - \frac{\delta W_2(\xi,\xi) + \delta W_{2c}(\xi,\xi)}{K(\xi,\xi)} \right\} \tag{30}$$

where both δW_{2c} and K now depend on the longitudinal component, $\xi_{\parallel}$, of the displacement vector.

To continue, we assume that $\gamma^2/\gamma_A{}^2 << \frac{\Gamma p_0}{B_0{}^2}$. This approximation (fast propagation of sound waves) holds close to marginal stability, but is in fact more generally valid for internal kink modes in typical Tokamaks. We then obtain a lowest approximation to $\xi_{\parallel}$ by setting $\delta W_{2c} = 0$.

Equation (30) for the growth rate now takes the form

$$\frac{3}{m^2}\frac{\gamma^2}{\gamma_A{}^2} = \max_{\xi_0} \left\{ \frac{\Lambda_m \left[\int_0^1 \alpha\, x^{m+1} \xi_0 dx\right]^2 - \int_0^1 x dx\, \delta q^2 \left[(x\xi_0')^2 + (m^2-1)\xi_0^2\right]}{\int_0^1 x dx \left[(x\xi_0')^2 + (m^2-1)\xi_0^2\right]} \right\} \qquad (31)$$

with Λ_m given by Eqn.(20).

For the m=1, n=1 internal kink mode this variational problem is analytically soluble for arbitrary profiles of the safety factor $\delta q(x)$, and pressure $p(x)$. The growth rate is given by

$$\Lambda_1 \int_0^1 \frac{dx}{x^3(\delta q^2 + 3\gamma^2/\gamma_A{}^2)} \left(\int_0^x \alpha(t) t^2 dt\right)^2 = 1 \qquad (32)$$

The growth rate obtained from Eqn. (32), including the variation over r_1, is compared in Fig 2 with growth rates obtained from the FAR initial value stability code[4,6]. The q profile in this case is $q=q_o+6.8(\frac{r}{a}-\frac{1}{2})^3$ for $r/a>\frac{1}{2}$ and $q=q_0$ for $r/a<\frac{1}{2}$; $\beta_o=0.66\%$ and $\varepsilon=0.1$. Also shown in Fig 3 is an improved analytic result. This was derived by expanding the

factor $\left(\frac{1}{q} - \frac{1}{2}\right) \simeq \frac{1}{2} - \delta q(r)$ in solving for the $m=2$ sideband, and retaining the first order corrections $0(\delta q)$ perturbatively. The improved agreement with the numerical growth rates suggests that this expansion is the main source of error in the analytic treatment. As has been indicated above the growth rate obtained from Eq. (32) with $x=r/r_1$ has been maximised with respect to variation of the parameter r_1/a. The dependence of γ on the choice of r_1 is shown in Fig 3. The procedure followed in solving equation (32) for γ is to choose a value of r_1 in the region where $(q-1)$ is small, calculate $\Lambda_1(r_1)$ (equation (20)) and the integral, to obtain $\gamma(r_1)$, and then to maximise $\gamma(r_1)$. Fig 3 shows the variation of $\gamma(r_1)$ for the same $q(r)$ profile as Fig 2, and with $q_0 = 1.004$.

4. Adiabatic compression during the sawtooth precursor.

Observations on JET[12] show that as the magnetic axis is displaced during the $m=1$, $n=1$ instability occurring just before the sawtooth temperature collapse, the peak electron temperature as measured by electron cyloctron emission (E.C.E.) may increase by a substantial amount. In one example[12] in which the plasma displacement was outward, along the E.C.E. line of sight the peak temperature T_{eo} was seen to increase from around 6.3 keV to 7.2 keV before the temperature crash. A possible explanation of this is that the temperature perturbation is caused by local adiabatic compression of the plasma. At marginal stability the plasma motion, as predicted by ideal MHD fluid equations, is strictly incompressible, but at finite growth rate we can calculate $\nabla \cdot \underset{\sim}{\xi}$ from

equation (30) by going to next order in $(\gamma^2/\gamma_A{}^2\beta_0)$. The result is

$$\nabla\cdot\xi \simeq 2\frac{\gamma^2}{\gamma_A{}^2}\frac{B^2}{\Gamma p}\frac{\xi_R}{R_0} \tag{33}$$

where ξ_R is the outward displacement from the symmetry axis. With growth rate taken from experimental observation of the 1/1 displacement[1] $(\gamma/\gamma_A \simeq 10^{-2})$ and the experimental value of $\beta \sim 10^{-2}$, this would yield an estimate for the temperature perturbation δT at the magnetic axis;

$$\delta T = -\frac{2}{3}(\nabla\cdot\xi)T_0 = -1.6\,\frac{\xi_R}{R}\frac{\gamma^2}{\gamma_A{}^2\beta_0}T_0 \tag{34}$$

of about 15eV for a 45cm displacement of the axis. This δT represents cooling due to adiabatic expansion where the axis is convected outward into the weaker toroidal magnetic field, and compressional heating where it is convected inward. In addition the magnitude of the perturbation falls far below the observed temperature increase of about 900eV.

However collisional fluid equations are clearly inadequate to describe compressional effects occurring on a time scale of 100 μ sec when the electron and ion collision times are of order 100 μ sec and 10 m sec respectively. The appropriate theory describes individual particle motion along the field and replaces the energy integrals of ideal MHD by the kinetic energy principle [7,8].

The only modification required in the foregoing calculation of stability boundaries and of growth rates, is the replacement of the compressional energy δW_{2c}, Eqn. (29) by the kinetic integral [7,8]

$$\delta W_{2K} = -\frac{1}{2} \sum_j m_j \int d^3x \int d^3v \frac{\delta f_j^2}{\frac{\partial F_0}{\partial \varepsilon}} \tag{35}$$

where the perturbed distribution functions for ions and electrons are determined by the bounce averaged Fokker-Planck equations, or in a collisionless plasma by the Vlasov equations [8] or use of the μ and J adiabatic invariants [7].

$$\left(\gamma - \frac{in\delta q}{\tau} - \nu\langle c\rangle\right)\delta f = -\gamma \frac{\partial F_0}{\partial \kappa} \langle v_\parallel^2 \underset{\sim}{nn}:\nabla\underset{\sim}{\xi} + \mu B(\nabla\cdot\underset{\sim}{\xi} - \underset{\sim}{nn}:\nabla\underset{\sim}{\xi})\rangle \tag{36}$$

where, $\kappa = \frac{1}{2} v^2$ is the energy per unit mass, $\underset{\sim}{n} = \underset{\sim}{B}/|B|$,

$$\tau = R_0 q \int \frac{d\theta}{|v_\parallel|} \tag{37}$$

is the transit time for passing particles, and is the bounce-time between turning points, for trapped particles.

$$\langle A\rangle = \frac{1}{\tau} \int \frac{R_0 q\, d\theta}{|v_\parallel|} A \tag{38}$$

is the orbit average of A, and the term $in\delta q/\tau$ on the left hand side of Equation (36) appears only for passing particles. An important feature of

this equation is that the right hand side becomes small, of order $(\varepsilon \frac{\xi_0}{R})$ for passing particles, while it is of order ξ_0/R for trapped particles and those passing particles with $v_\parallel/v \sim 0(\varepsilon^{1/2})$, which we shall refer to as 'slow passing' particles. This arises because the quantities $\nabla\cdot\underset{\sim}{\xi}$, and $\underset{\sim}{nn}:\nabla\underset{\sim}{\xi}$ are oscillatory ($\propto \cos\theta$) in leading order, and couple to the variation of $|B|$ and $v_\parallel$ in the orbit averages. As a result the energy integral, Eqn.(35) can only have a contribution of order $\varepsilon^2(\xi_0{}^2/R^2)$ from passing particles, while the slow-passing and trapped particles contribute $\varepsilon^{1/2}(\xi_0{}^2/R^2)$. The precise nature of the solution in this region of velocity space depends on the relative magnitude of three frequencies: ν_j/ε, the effective collision frequency for slow particles $(\frac{v_\parallel}{v} \sim \varepsilon^{1/2})$; τ_b^{-1}, the bounce or transit frequency for slow particles; and γ, the growth rate. In the following we consider three limiting cases as examples

(a) collisionless limit ($\nu \to 0$) with $\gamma\tau \ll \delta q$

(b) collisionless limit ($\nu \to 0$) with $\gamma\tau \gg \delta q$

(c) collisional limit: $\nu \gg \gamma \gg \delta q/\tau$.

In the third case the collision operator is taken to have the Lorentz form, appropriate for electrons if $Z_{eff} \gg 1$. The perturbed distribution is then forced to be isotropic, but not necessarily Maxwellian.

The relevant solutions for δf for these cases are:

$$\text{(a)}\quad \delta f = \frac{m\kappa}{T}\lambda B_o \frac{\xi_r}{R} \langle \cos\theta \rangle F_m \qquad \text{Trapped particles}$$

$$= \quad 0 \qquad \text{Passing particles} \qquad (39a)$$

$$\text{(b)}\quad \delta f = \frac{m\kappa}{T}\lambda B_o \frac{\xi_r}{R} \langle \cos\theta \rangle F_m \qquad \text{all particles} \qquad (39b)$$

$$\text{(c)}\quad \delta f = \frac{m\kappa}{T}\frac{\xi_r}{R} F_m \sqrt{2\varepsilon}\, h \qquad \text{all particles} \qquad (39c)$$

$$h = \frac{1}{2\pi}\int_0^1 dm\,(2E-K) + \frac{1}{\pi}\int_0^1 \frac{dm}{m^{3/2}}\left(\frac{2(E-K)}{m} + K\right) \equiv 0.099 \qquad (40)$$

where $E(m)$ and $K(m)$ are the complete elliptic integrals, and we have introduced the pitch angle variable $\lambda B = v_\perp^2/v^2$.

Inserting the appropriate solution for δf into the kinetic integral, Eqn. (35), we obtain:-

$$\delta W_{2K} = 2\pi^2 R_0 B_0^2 \int_0^{r_1} r\,dr\, \frac{15}{8\pi}\frac{p}{B_0^2}\frac{|\xi_{ro}|^2}{R_0^2}\left(\frac{2r}{R_0}\right)^{1/2}\mu \qquad (41)$$

where the numerical coefficient, μ, which results from pitch angle integration over bounce averaged quantities, is given by

$$\mu = 2\int_0^1 dm\,\frac{(2E-K)^2}{K} = 1.108\,, \qquad \gamma\tau_b \ll \delta q,\ \nu \to 0 \qquad (42a)$$

$$\mu = 1.108 + 2\int_0^1 \frac{dm}{m^{3/2}K}\left[K + \frac{2}{m}(E-K)\right]^2 = 1.292 \ , \quad \gamma\tau_b >> \delta q, \quad \nu \to 0 \qquad (42b)$$

$$\mu = 2\pi h^2 (2r/R)^{1/2} = 0.09\sqrt{\varepsilon} \ , \qquad \nu >> \gamma >> \delta q/\tau b \qquad (42c)$$

In case, (a) only trapped particles contribute and the coefficient μ is the same as that found by Antonsen, Lane and Ramos [13] for a similar (interchange) stability problem. In the second case, (b) the slow passing particles also contribute but are seen to be much less important than the trapped particles. The discontinuity which appears in δf when $\gamma\tau_b << \delta q$ is resolved by a collisional boundary layer of width $(\frac{\nu}{\gamma})^{1/2}$ but this does not affect the energy integrals significantly. In case (c) pitch angle scattering has smoothed the perturbed distribution function to be isotropic and has reduced the magnitude of the kinetic term.

The inclusion of this stabilising effect has two interesting consequences. Firstly, ultra-flat $q(r)$ profiles may be stable to the ideal $m=1$, $n=1$ mode even when $\delta q(x) \equiv 0$, and no field line bending energy is available to balance the pressure gradient driving terms. This could explain observations on JET [14] which suggest that a $q=1$ surface exists during the ramp phase of the sawtooth.

Secondly, the kinetic compression term, Eqn. (35), indicates that a substantial increase in temperature should occur as the magnetic axis is displaced by the $m=1$, $n=1$ motion. Equation (41) suggests that the pressure perturbation $\frac{\delta p}{p} \sim \varepsilon^{1/2}\frac{\xi_0}{R}$ rather than $0(\frac{\gamma^2}{\gamma_A{}^2\beta}\frac{\xi_0}{R})$ found in

collisional theory (Eqn. 34). However, equation (41) conceals the fact that the pressure perturbation in collisionless theory is anisotropic. To interpret the E.C.E. measurements correctly one must return to the perturbed (anisotropic) electron distribution function and calculate the radiation temperature, T_r [15]

$$T_r = - \frac{m \int \eta_\omega f d^3v}{\int \eta_\omega \frac{1}{v_\perp} \frac{\partial f}{\partial v_\perp} d^3v} \tag{43}$$

where $\eta(\omega, v, \theta)$ is the emissivity. Considering emission perpendicular to the magnetic field and taking the non-relativistic limit, $\eta \alpha v_\perp^2$ equation (43) for T_r becomes

$$T_r = - \frac{m \int_0^\infty \kappa^{3/2} d\kappa \int_0^{1/B} \frac{B d\lambda}{\sqrt{1-\lambda B}} \lambda B \left[F_m(\kappa) + \delta f(\lambda, \kappa) \right]}{\int_0^\infty \kappa^{3/2} d\kappa \int_0^{1/B} \frac{B d\lambda}{\sqrt{1-\lambda B}} \lambda B \left(\frac{\partial}{\partial \kappa} + \frac{1}{\kappa B} \frac{\partial}{\partial \lambda} \right) \left[F_m + \delta f \right]} \tag{44}$$

Equation (44) may be expanded for small ξ_r/R to give an expression for the perturbed radiation temperature T_r.

The result depends sensitively on the degree of anisotropy of δf. Taking the distributions of (39b) and (39c) as examples δT_r may be calculated explicitly in terms of elliptic integrals. The results are

$$\delta T_r / T_e = 1.1 \sqrt{\frac{R}{r}} \frac{\xi_r}{R}, \qquad \gamma\tau >> \delta q; \quad \nu_e \to 0 \quad \text{and} \quad \theta = \pi \tag{45b}$$

$$\delta T_r/T_e = 0.09\sqrt{\frac{r}{R}}\,\frac{\xi_r}{R}, \qquad \nu_e > \gamma > \delta q/\tau \tag{45c}$$

Initially there are no trapped electrons at the magnetic axis since $\nu_* = \frac{\nu_e R}{v_{Te}}\left(\frac{R}{r}\right)^{3/2} \to \infty$ there. As the axis is displaced into a helix by the $m = 1$ instability $\nu_* < 1$ is satisfied when $\xi/R \approx (\nu_e R/v_{Te})^{2/3}$. At this point banana regime dynamics begins to apply and the appropriate equations governing $T_r(t)$ are obtained by setting $r \to \xi_r$, so that

$$\frac{1}{T_{eo}}\frac{d}{dt}T_r \approx 2.2\,\frac{d}{dt}\left(\frac{\xi_r}{R}\right)^{1/2} \tag{46.b}$$

and

$$\frac{1}{T_{eo}}\frac{dT_r}{dt} \approx 0.06\,\frac{d}{dt}\left(\frac{\xi_r}{R}\right)^{3/2} \tag{46.c}$$

for the two cases considered above.

Taking $\xi_r/R \sim 1/6$ and $T_{eo} = 6.3$keV the resulting estimates for δT_r are >5keV, and 25eV respectively. A very sharp transition therefore occurs when the growth rate γ exceeds the 90° Coulomb scattering frequency ν_e. In practice at 6.3keV, with $Z_{eff} \sim 3$, $\nu_e^{-1} \sim 100\,\mu$sec in the JET discharge for which a 900eV temperature increase was recorded. This is comparable to the growth time so it is not surprising that the observation is intermediate between the extremes predicted by (46b) and (46c). At somewhat lower electron temperature the more collisional result

of (46c) should hold which may account for the fact that significant increases in the E.C.E. radiation temperature are unusual.

5. Stability Boundaries in the Banana Regime.

To determine the ideal MHD stability boundaries of internal kink modes in the banana regime the compressional energy, Eqn. (41), must be added to the field line bending energy and pressure gradient terms of the energy integrals in Eqn. (14). Of the three coupled Euler equations (16)-(18) which are obtained from the variational problem of minimising δW, only equation (16) is modified, so that after elimination of the two sideband displacements, the eigenvalue equation becomes:-

$$\frac{d}{dx}\left\{x^3\left[\delta q^2+3\gamma^2/\gamma_A^2\right]\frac{d\xi_o}{dx}\right\} - \xi_0 x(m^2-1)\delta q^2 + \alpha x^{m+1}\Lambda_m\int_o^1 \alpha\, x^{m+1}\xi_0 dx$$

$$- \frac{15}{8\pi}\mu\frac{p}{B_0^2}\left(\frac{2r_1}{R}\right)^{1/2} x^{3/2}\xi_0 = 0 \qquad (47)$$

We consider first the limit in which both electrons and ions may be treated as collisionless, and equation (39a) for δf applies.

Equation (47) has been solved for the $m=1$ mode. The transition out of the banana regime as $x\to 0$ was simulated by taking

$$\mu = \frac{1.1}{1 + \nu_* / x^{3/2}}$$

where $\nu_* = (\nu_{ei} R/\varepsilon_1^{3/2} v_{Te})$ is the usual collisionality parameter. With ν^* taken to be 1/80, Fig 4 shows the ideal stability boundary as a function of q_o and β_o. The aspect ratio A=3, the q profile used is the same as that for Fig 2 and the pressure profile is $p=p_o(1-r^2/a^2)^2$. Also shown in Fig 4 for reference is the marginal stability boundary for the collisional MHD limit in which the trapped particle stability term is absent in Eq.47; the strong stabilising effect of trapped particles is evident.

In practice, although the collisionless limit provides a good approximation for the ions, it does not for the electrons. The detrapping frequency for the electrons, ν_e/ε, typically exceeds the growth rate of the helical instability in JET, and even the 90° scattering frequency ν_e can be comparable with γ if $Z_{eff}>1$. The isotropising effect of collisions decreases the compressional stabilization for the electrons from $\varepsilon^{1/2}\beta_e$ to $0.1\varepsilon\beta_e$, (Eq. 42) and a much weaker stabilisation results.

6. Summary and Discussion.

An analytic theory has been presented for the m=1, n=1 ideal internal kink mode in equilibria with ultra-flat profiles of the safety factor q(r) in the core region. This extends the theory of Bussac et

al.[3]to a new regime in which $|q-1| \approx 0(\varepsilon)$ in the core. The theory also permits analysis of higher m,n modes with $m/n = 1$. Analytic expressions have been obtained for the eigenfunctions (equation (23)), the marginal stability criteria (equations (21),(26) and (27)) and linear growth rates (equation (32)). For the case of the 1/1 mode the analytic growth rates have been compared with numerical results from the FAR code and found to be in fairly close agreement.

The equations used in sections 1-3 are the collisional MHD fluid equations. A number of predictions from these equations are at odds with experimental observations. In the first place, ideal mhd theory predicts that 1/1 instability is inevitable if $q = 1$ at some radius (and is ultra-flat in the core region). This is in conflict with recent observations on JET[2,14] which suggest that (i) the $q(r)$ profile is very flat and close to unity in the core, (ii) $q(r_1) = 1$ at some radius throughout the sawtooth ramp phase.

In addition calculation of the heating (cooling) to be expected by adiabatic compression (expansion) during the linear phase of the 1/1 ideal kink mode predicts a 15eV drop in the electron temperature of the magnetic axis where it is convected outward from the symmetry axis. Experimentally a 900eV increase in the electron temperature has been measured from electron cyclotron emission during such a displacement [12]. In section 4 it was then shown that, for a plasma in the Banana regime of collisionality, important trapped particle terms must be included in the mhd stability analysis and that the anisotropic perturbation of the electron distribution function predicted by banana-regime dynamics can

result in a substantial increase in the radiation temperature as measured by E.C.E. A second important consequence of low-collisionality dynamics is that the ideal 1/1 mode may be completely stabilised, (Eqn. 48) even when $q(r)$ passes through unity and is ultra-flat in the core.

We conclude from these results that the fluid MHD model has serious limitations when detailed comparisons with sawtooth data are attempted. Trapped particle effects, which were previously investigated in connection with interchange [13,16] and high-n ballooning modes [17], may be distinguished in the behaviour of the $m=1$, $n=1$ instability preceding the temperature collapse in the sawtooth.

Acknowledgements.

We are indebted to Dr. D.J. Campbell for the opportunity to study the E.C.E. data (reference 12) prior to publication and for discussions, to T.J. Martin for the computation of the coefficients μ(Eqns. (41) and (42)) and to P. Kirby and J. Wesson for stimulating discussions. We are also indebted to the Oak Ridge MHD group for providing us with an original version of the FAR code.

References.

[1] Edwards, A.E., et. al. Phys. Rev. Letts. 57, 210 (1986)

[2] Wesson, J.A., Kirby, P., Nave, F., Plasma Physics and Controlled Nuclear Fusion Research Proc. 11th International Conf. Kyoto 1986)

[3] Bussac, M.N., Pellat, R., Edery, D., Soulé, J.L., Phys. Rev. Letts. 35, 1638, (1975)

[4] Hastie, R.J., Hender, T.C., Carreras, B.A., Charlton, L.A., Holmes, J.A., to be published in Phys. Fluids

[5] Wesson, J.A., Plasma Physics and Controlled Fusion 28, 243 (1986)

[6] Hender, T.C., Hastie, R.J., and Robinson, D.C., Culham Lab. Preprint CLM-P794 (1987) (To appear in Nucl. Fusion); and Charlton, L.A., Holmes, J.A., Hicks, H.R., Lynch, V.E. and Carreras, B.A., Journal of Comp. Physics., 63, 107 (1986).

[7] Kruskal, M.D., Oberman, C.R., Phys. Fluids 1, 275 (1958)

[8] Rosenbluth, M.N., Rostoker, N., Phys. Fluids 2, 23 (1959)

[9] Connor, J.W., Hastie, R.J., CLM-M106, (1985)

[10] Kirby, P. Culham Lab. Preprint (1987) CLM-P809.

[11] Bernstein, I.B., Freeman, E.A., Freeman, M.D., Kruskal, M.D., Kulsrud, R.M., Proc. Roy. Soc. A244, 17(1958)

[12] Campbell, D.J., private communication.

[13] Antonsen, T.M., Lane, B.A., Ramos, J.J., Phys. Fluids 24, 1465 (1981).

[14] Weller, A., et al., to be published.

[15] Bekefi, G., Radiation Processes in Plasmas, Wiley and Sons, N.Y., 1966.

[16] Connor, J.W. and Hastie, R.J., Phys. Rev. Lett. 33, 202 (1974).

[17] Rutherford, P., Chen, L., and Rosenbluth, M.N., Princeton report PPPL-1418 (1978).

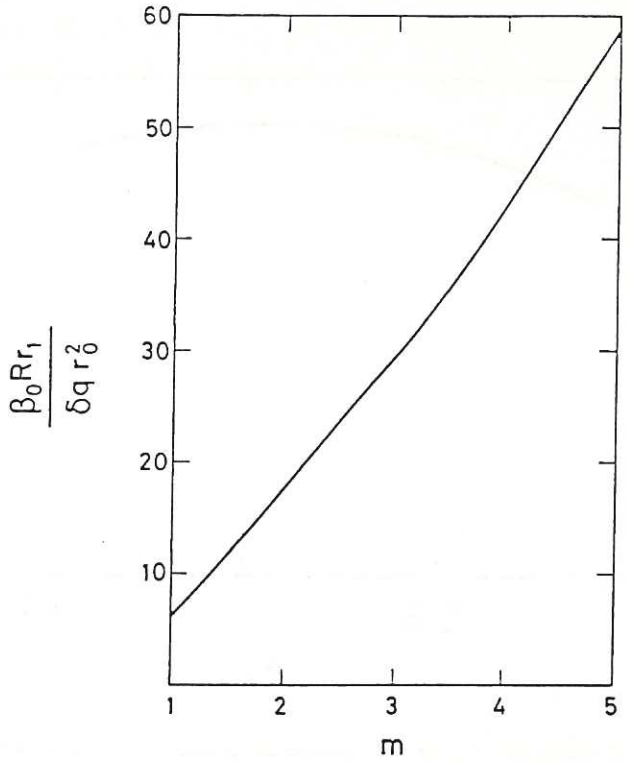

Fig 1. Threshold β_0 value as a function of mode number m calculated from Equation (27). Equilibrium $p=p_0(1-\frac{r^2}{r_0^2}$; $q = 1+\delta q$ = constant $(r<r_1)$; $q = 1+\delta q + 3(\frac{r-r_1}{a})^2$; $(r_1<r<a)$ with $r_1/a = 1/3$.

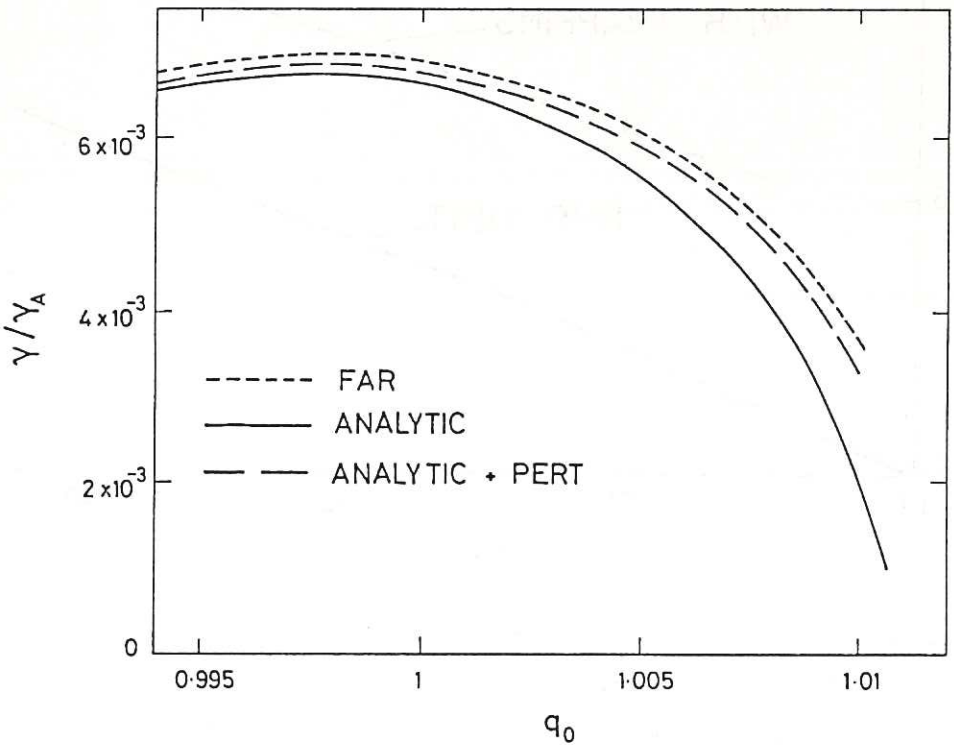

Fig 2. Comparison of analytic growth rates with numerical values obtained from the initial value code FAR. Solid line is obtained from Equation (32). The broken analytic line introduces small corrections perturbatively by expanding $(\frac{1}{q}-\frac{1}{2}) = \frac{1}{2} - \delta q(r)$ in solving for the m=2 sideband (see text). Equilibrium $q=q_0$, $r/a < 0.5$; $q=q_0 + 6.8(r/a - 0.5)^3$, $r/a > .5$. $\beta_0 = 0.66\%$, $a/R = 0.1$.

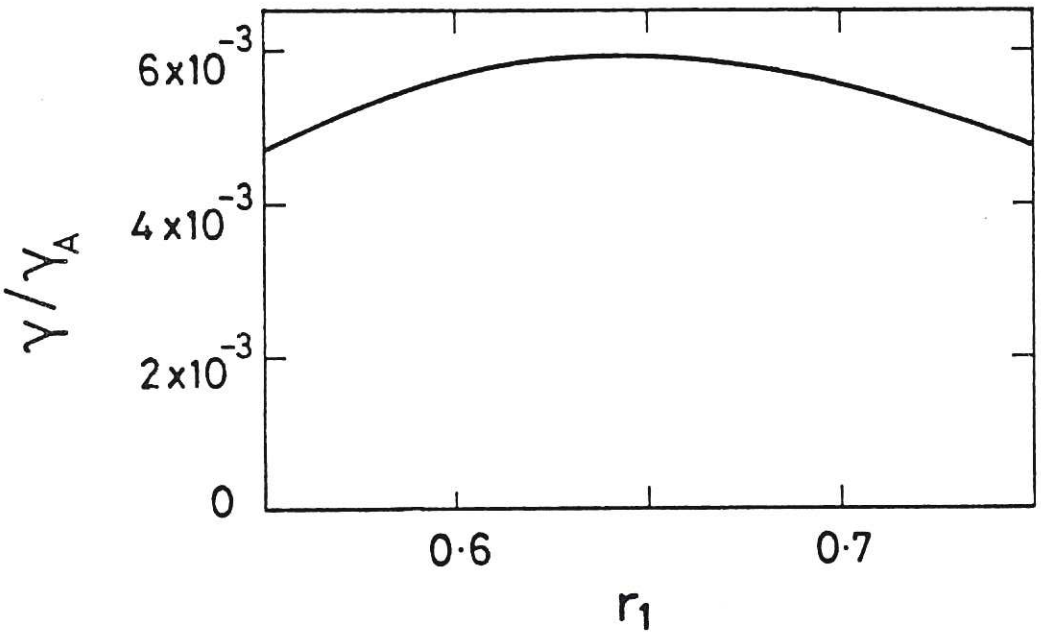

Fig 3. Effect of varying r_1 on the analytic growth rate obtained from Equation (32). Same profile as Fig 2 with $q_0 = 1.004$.

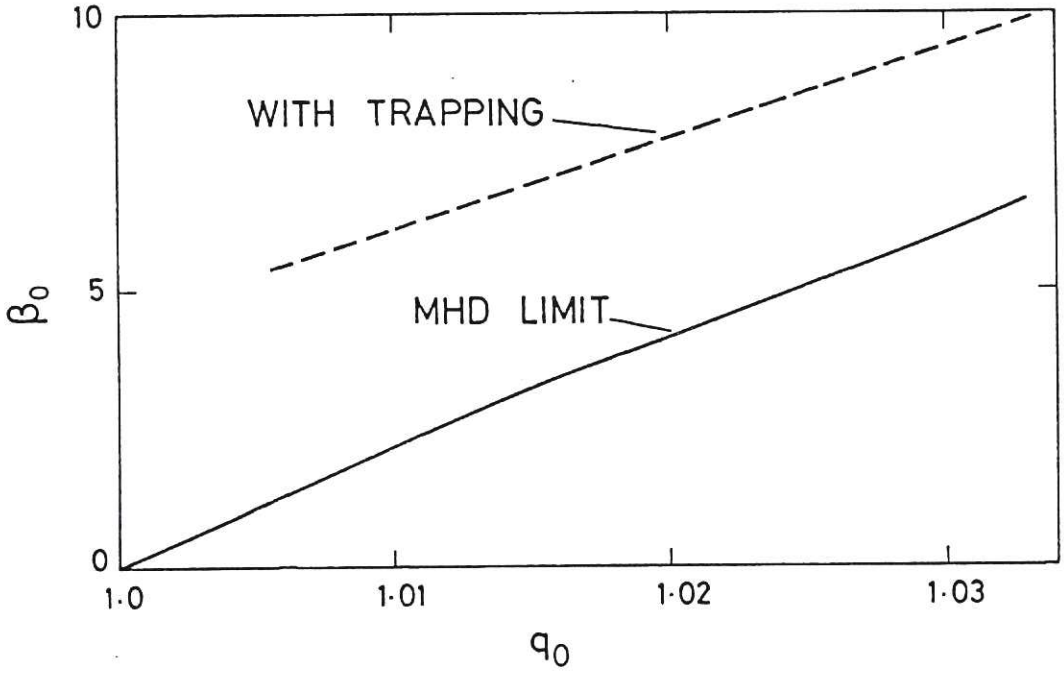

Fig 4. Effect of trapped particle stabilisation on the stability boundary of the m=1, n=1 mode. Solid curve is the boundary in the absence of trapped particles. The broken curve shows the effect of trapping. q profile as in Fig 2, $p=p_0(1-r^2/a^2)^2$, aspect ratio A = 3.